CONVERGENCE PROPERTIES OF A DIAKOPTICS METHOD FOR ELECTROMAGNETIC SCATTERING FROM 3-D COMPLEX STRUCTURES

V. Lancellotti* and A. G. Tijhuis

Faculty of Electrical Engineering, Eindhoven University of Technology, Den Dolech 2, 5600 MB Eindhoven, The Netherlands

Abstract—Linear embedding via Green's operators (LEGO) is a diakoptics method that employs electromagnetic "bricks" to formulate problems of wave scattering from complex structures (e.g., penetrable bodies with inclusions). In its latest version the LEGO integral equations are solved through the Method of Moments combined with adaptive generation of Arnoldi basis functions (ABF) to compress the resulting algebraic system. In this paper we review and discuss the convergence properties of the numerical solution in relation to the number of ABFs. Besides, we address the issue of setting the threshold for stopping the generation of ABFs in conjunction with the adaptive Arnoldi algorithm.

1. INTRODUCTION

Electromagnetic (EM) scattering problems are usually formulated in the frequency domain by means of coupled integral equations (IE), since in this way the radiation conditions at infinity are intrinsically accounted for by the relevant Green's function of the background medium [1]. The downside with IEs is that, when they are reduced to a weak form through the baseline Method of Moments (MoM) [2], they lead to algebraic systems with densely populated matrices. Furthermore, if the structure of concern spans many wavelengths, then most likely the resulting matrix is also large, and hence can only be inverted with iterative methods.

To alleviate this shortcoming one can resort to diakoptics [3], which nowadays is also known as domain decomposition. In words, diakoptics is the conceptual separation of a complicated problem

into "small" parts which are first characterized as independently as possible. The original problem is then rigorously reconstructed upon combining the various parts in a consistent manner. Among the methods that fit this description are (list is definitely incomplete): the Synthetic Function Expansion [4], the Characteristic Basis Functions Method [5], the Equivalence Principle Algorithm [6], the Generalized Surface Integral Equation method [7], and Linear Embedding via Greens Operators (LEGO), developed by these authors [8, 9].

In the framework of LEGO a complicated structure (see Fig. 1) is modelled as a combination of sub-domains (EM bricks). Although in principle no restrictions exist as to the shape and to the content of the bricks, handling arbitrary occurrences in practice is not trivial. In fact, recently we extended the LEGO method to allow for bricks with different content [10, 11]. At any rate, the original EM scattering problem is formulated through a set of coupled IEs for the unknown equivalent current densities which are introduced on the bricks' surfaces. The algebraic system that ensues by applying the MoM is compressed by using a set of Arnoldi basis functions (ABFs) [9] which are in turn expressed in terms of the underlying Rao-Wilton-Glisson basis functions (RWG) associated with the triangular-faceted mesh.

Normally the ABFs (needed to accurately compute the current densities) are far fewer than the RWGs introduced at the beginning. However, estimating beforehand the number n_A of ABFs that a specific problem will actually require is not trivial and may not be feasible at all under general circumstances. For this reason, by solving diverse scattering problems [10–14], we studied the dependence of n_A (for a given level of accuracy) on various parameters. The numerical experiments led us to identify distinctive trends of the convergence patterns in relation to geometrical and physical parameters of the structures under investigation. However, expressing these behaviors collectively in a simple mathematical formula (that yields n_A) seems hardly possible. Therefore, from a practical standpoint, we find it convenient to generate the ABFs adaptively at an additional yet affordable computational cost, as we showed in [11].

For ease of reference in this paper we review and collect the main results on convergence obtained heretofore. We also extend the set of available "rules of thumb" by discussing a new convergence study that involves bricks with different content. Besides, in conjunction with the adaptive Arnoldi algorithm [11], we address the issue of setting the threshold for stopping the generation of ABFs.

The rest of the paper is organized as follows. In Section 2 we outline the formulation of a scattering problem with LEGO, whereas in Section 3 we describe the numerical strategy. In Section 4.1 we provide
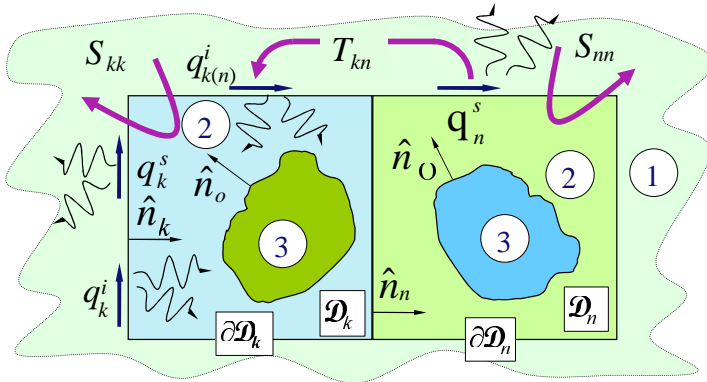
Figure 1. For illustrating diakoptics with LEGO: bricks $\mathcal{D}_k$, $\mathcal{D}_n$ are shown along with related operators and equivalent symbolic surface currents. In this setup the background medium ①, the host medium ② and the object ③ may *all* have different properties; media ② and ③ need not be the same for all bricks (cf. [9]).

a simple example of validation of the LEGO code. The convergence properties of the numerical solution with ABFs are presented in Section 4.2 and discussed in Section 4.3. Eventually, the choice of the threshold for the adaptive Arnoldi algorithm is discussed through a numerical example in Section 4.4.

2. PROBLEM FORMULATION WITH LEGO

The procedure for formulating a 3-D scattering problem with LEGO [9] consists of the following main steps (Fig. 1):

(i) conceptual separation of the structure into "small" parts (i.e., diakoptics properly said) which are "enclosed" in simple-shaped domains (EM bricks) $\mathcal{D}_k$, $k = 1, \ldots, N_D$;

(ii) description of the EM behavior of $\mathcal{D}_k$ through scattering operators S_{kk}; this is accomplished *separately* for each brick type;

(iii) accounting for the multiple scattering that occurs between $\mathcal{D}_k$, $\mathcal{D}_n$ by means of transfer operators T_{kn}, $n \neq k$;

(iv) combination of the bricks in an EM sense in order to accomplish the description of the original problem.

Unlike the assumption made in [9], however, in this work we allow for bricks with possibly different content. Nonetheless, we suppose the

bricks all possess the same shape, although strictly speaking this is not required for diakoptics.

All the geometrical details (i.e., size and shape of the inclusions, if any are present) and the material complexities (e.g., inhomogeneous constitutive parameters) within $\mathcal{D}_k$ are rigorously captured by S_{kk}. To this purpose, we invoke the surface equivalence principle in the form of Love [15] to define suitable equivalent problems along with the corresponding unknown electric ($\mathbf{J}$) and magnetic ($\mathbf{M}$) surface current densities over $\partial \mathcal{D}_k$. As a result, S_{kk} (which carries information solely about a brick's content) tells how an impinging wave is reflected back, namely [8, 9],

$$q_k^{\mathrm{s}} = \mathsf{S}_{kk} q_k^{\mathrm{i}}, \quad q^{\mathrm{s,i}} = \begin{bmatrix} \sqrt{\eta_1} \mathbf{J}_k^{s,i} \\ -\mathbf{M}_k^{s,i}/\sqrt{\eta_1} \end{bmatrix}, \quad \eta_1 = \sqrt{\frac{\mu_1}{\varepsilon_1}}, \tag{1}$$

where the superscript s (i) denotes scattered (incident) equivalent current densities on $\partial \mathcal{D}_k^-$, with the positive (negative) side of $\partial \mathcal{D}_k$ specified by the positive (negative) sense of the normal $\hat{\boldsymbol{n}}_k$. Besides, the currents $\mathbf{J}_k^{\mathrm{s,i}}$, $\mathbf{M}_k^{\mathrm{s,i}}$ are placed against $\partial \mathcal{D}_k$, but "live" within the background medium ①, as Fig. 1 suggests†.

The actual calculation of S_{kk} requires solving the boundary value problem in $\mathcal{D}_k$ via suitable IEs, the number and nature of which are determined by the brick's content. For the sake of argument, if medium ① and ② are just the same, so that $\partial \mathcal{D}_k$ represents no more than a mathematical boundary, then the functional equation yielding S_{kk} is [8, Eq. (11)]. More generally, if $\partial \mathcal{D}_n$ is a material interface, then S_{nn} obtains through the formal cascade of the scattering operator of the interface, $\bar{\mathsf{S}}_{\mathrm{J}n}$, and the operator of the inner part, $\mathsf{S}_{\mathrm{L}nn}$, [9, Eqs. (2), (3)]. A special case of the previous one occurs when no inclusion is contained in $\mathcal{D}_n$; then, $\mathsf{S}_{\mathrm{L}nn} = 0$, and S_{nn} reduces simply to $\bar{\mathsf{S}}_{\mathrm{J}11,n}$ [9, Eq. (A4)].

The transfer operator T_{kn} accounts for the additional incident currents on $\mathcal{D}_k$ that develop in response to the scattered currents on $\mathcal{D}_n$, as exemplified in Fig. 1. The relevant IEs and current definitions read [9]

$$q_{k(n)}^{\mathrm{i}} = \mathsf{T}_{kn} q_n^{\mathrm{s}}, \qquad q_{k,\mathrm{tot}}^{\mathrm{i}} = q_k^{\mathrm{i}} + q_{k(n)}^{\mathrm{i}}, \qquad n \neq k, \tag{2}$$

where the subscript '$k(n)$' signifies "contribution on $\partial \mathcal{D}_k^-$ due to $\mathcal{D}_n$." Notice that T_{kn} is only affected by the position and shape of the bricks in the model. Furthermore, for problems which exhibit even a limited translational symmetry, the transfer operators come in groups

---

† In actuality, this carefulness becomes unnecessary when $\partial \mathcal{D}_k$ represents a mathematical surface [8], because then the distinction between $\partial \mathcal{D}_k^+$ and $\partial \mathcal{D}_k^-$ is an inessential one.

of identical elements [8]. This may result in a substantial reduction of both computational time [8, 12] and memory occupation, since only one specimen belonging to each class must be computed and stored.

Now, the two systems of N_D IEs that govern the EM behavior of the original structure (illuminated by an external incident wave) can be stated upon combining (2) and the first of (1) with q_k^i replaced by $q_{k,\text{tot}}^i$. Specifically,

$$(\mathsf{I} - \mathsf{T}\,\mathbf{diag}\{\mathsf{S}_{kk}\})q_{\text{tot}}^i = q^i, \quad q^s = \mathbf{diag}\{\mathsf{S}_{nn}\}q_{\text{tot}}^i, \tag{3}$$

with $(q_{\text{tot}}^i)_k = q_{k,\text{tot}}^i$, $(q^i)_k = q_k^i$ and T an $N_D \times N_D$ symbolic matrix of transfer operators [9, Eq. (6)]. Once the first of (3) has been solved numerically, as outlined in Section 3, we can compute the scattered fields—which are radiated by the currents q^s—as well as the total (twisted) tangential fields over the bricks' surfaces through $q_{\text{tot}}^i - q^s$.

3. NUMERICAL SOLUTION (OUTLINE)

The inversion of (3) begins with the baseline MoM employed in combination with sub-domain RWG basis functions in order to obtain the algebraic counterpart of the scattering and transfer operators, viz., $[S_{kk}]$, $[T_{kn}]$. The corresponding weak forms of (3) are linear systems of rank $2N_F N_D$, $2N_F$ being the number of RWG functions used to expand $\mathbf{J}_k^{s,i}$ and $\mathbf{M}_k^{s,i}$ [8, Eq. (20)]. Concerning this, the two non-null $N_F \times N_F$ sub-blocks of $[T_{kn}]$ are obtained in a low-rank factorized form [9, Eq. (11)] by commingling the calculation of (few) matrix entries with the adaptive cross approximation (ACA) [16]. This expedient (together with the additional memory saving brought in by the translational symmetry, when present) enables us to store comparatively large system matrices and hence, to tackle larger scattering problems.

As a final step toward the solution of (3) we compress the system matrix $([I] - [T]\mathbf{diag}\{[S_{nn}]\})$ by introducing a set of orthonormal vectors $[\psi_s]$, $s = 1, \ldots, n_A$, to represent the unknown coefficient, i.e.,

$$[q_{\text{tot}}^i] = [\Psi_{n_A}][a], \quad [\Psi_{n_A}] = [[\psi_1] \ldots [\Psi_{n_A}]]. \tag{4}$$

The $[\psi_s]$'s are computed by applying the Arnoldi iteration to the sequence $\{([T]\mathbf{diag}\{[S_{nn}]\})^{s-1}[q^i]\}_{s=1}^{n_A}$. As a byproduct one also gets an upper Hessenberg matrix $[H_{n_A}]$ which essentially *is* the reduced system matrix [9, Eq. (18)]. The $2N_F N_D$ elements of $[\psi_s]$ define macro functions over $\cup_{k=1}^{N_D}\partial\mathcal{D}_k$, when associated with the underlying RWGs. Thereby, it seems convenient to refer to $[\psi_s]$ as Arnoldi basis functions (ABFs) for short.

Last, in [11] we proposed an adaptive Arnoldi algorithm which quits generating ABFs the moment the relative incremental difference

$$\delta_a(n_A) \overset{def}{=} \frac{\| \, [q_{\text{tot}}^{\text{i}}](n_A) - [q_{\text{tot}}^{\text{i}}](n_A - 1) \, \|_2}{\| \, [q_{\text{tot}}^{\text{i}}](n_A) \, \|_2} = \frac{\left\| [a_{n_A}] - \begin{bmatrix} [a_{n_A-1}] \\ 0 \end{bmatrix} \right\|_2}{\|[a_{n_A}]\|_2}, \quad (5)$$

has become smaller than a given threshold. Although (5) requires solving the (reduced) algebraic system on the fly after each new ABF is added to the growing set, the extra computational burden is worthy, as the procedure prevents calculating unnecessary higher-order ABFs.

4. NUMERICAL RESULTS

Implementing the occurrence of bricks with different content in a new code was not trivial, even though we could re-utilize large parts of the previous ones [8, 9]. For instance, the routines that calculate $[S_{kk}]$ and $[T_{kn}]$ via integral equations and MoM (Section 3) need not be updated, as this step of the method's stays the same regardless of the actual form of (3). Nonetheless, handling more than one type of bricks entails describing the model (i.e., stating what types of and how many bricks are there) and loading this data tidily. What's more, in view of the complexity of [9, Eqs. (15), (16)], care must be exercised while generating the ABFs.

4.1. Example of Validation

As a sanity check, in [10] we made sure the results yielded by the new code agreed with the ones provided by the old one, in the special case of bricks all having the same content (PEC objects). In addition, we provide an example of validation based on the toy problem shown in Fig. 2.

The structure (a dielectric slab in which two cylindrical holes with different radii have been excised) lends itself to being modelled and simulated in at least two ways: a) as a single brick, for which the old code can be used; b) by means of two bricks of different type, an instance that only the new code handles. The data relevant to this scattering problem are given in Fig. 2, whereas the details of the two bricks are outlined with the aid of Fig. 3. The number of ABFs for the two-brick model was set to $n_A = 70$ (corresponding to a threshold $\delta_a(n_A) = 10^{-15}$), whereas the total size of the original system is $2N_F N_D = 2304$. As the radar cross sections (RCS) computed with the foresaid strategies (also shown in Fig. 2) are in excellent agreement, this

experiment confirms the reliability of the new code, since the previous
one was thoroughly validated against the MoM in [9].

4.2. Convergence of ABFs: Analysis

Obtaining the ABFs may stand as the most time-consuming part
of the numerical strategy. Therefore, it is expedient to investigate
how the geometry and the material properties of a structure affect
the convergence rate of the current coefficients a_s [see (4)] and
ultimately, the number n_A of ABFs necessary for a given level
of accuracy. Regarding this, the effect of geometrical variables
(e.g., number, position and distance of the bricks) and certain
combinations of material properties and frequency were already
addressed elsewhere [11–13]: For quick reference we summarize the
main results hereafter, while wittingly omitting data not really
conducive to the discussion of Section 4.3. The Reader interested in
the geometrical and physical parameters of the simulations as well as in
knowing what the actual convergence patterns look like, is advised to
consult the pertinent papers. Finally, in what follows, it is understood
that n_A means "the number of ABFs required to achieve a given value
of $\delta_a(n_A)$".

Number of bricks The solution of (electrically) larger problems
   usually requires a larger number of ABFs. This expectation was
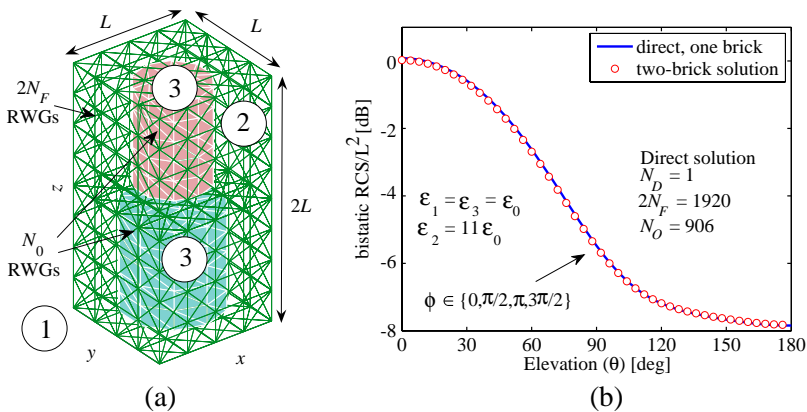
Figure 2. For LEGO validation: (a) simple dielectric structure with
cylindrical holes; (b) the bistatic RCS yielded by the new code ($\circ$)
is compared to the results computed with the previous version of
the code ($-$). *Data*: $f = 4\,\text{GHz}$, $\mathbf{E}^i = (\hat{\mathbf{y}} + j\hat{\mathbf{x}})\exp(-jk_1z)\,[\text{V/m}]$,
$k_1 = 2\pi f\sqrt{\varepsilon_1\mu_0}$. See Fig. 3 for remaining data.

confirmed by analyzing structures modelled with an increasing number of identical bricks arranged in a rectangular pattern [12]. In particular, PEC and dielectric spheres embedded in a dielectric host medium were considered [12, Fig. 3]: n_A is seen to grow with N_D [12, Fig. 5]. Thanks to the same set of experiments we also found out that, for the same number and arrangement of the bricks, the convergence is faster when the spheres are dielectric rather than PEC [12, Fig. 5].

Host-medium permittivity Finite-size dielectric slabs of ever increasing permittivities (i.e., medium ② in Fig. 1) with spherical PEC inclusions arranged in a regular pattern were described in [13, Fig. 2]. The convergence pattern of a_s plotted in [13, Fig. 6] shows that n_A grows as the contrast ratio $\varepsilon_2/\varepsilon_1$ is increased.

Shape and size of the inclusions In [13] we also investigated the influence of the geometry of the inclusions on the coefficients a_s. To this purpose, cubic bricks containing PEC objects of different size and shape (i.e., cones and prisms) were combined to model a rectangular finite-size dielectric slab [13, Fig. 3] in line with the LEGO philosophy. The outcome is that n_A increases if the objects are either larger or possess sharp corners [13, Fig. 7].

Presence of inclusions Making use of the scattering operator of a material interface introduced in [9], it was possible to model a composite dielectric slab comprised of a stack of four materials with different permittivities (ε_2) and no inclusions [13, Fig. 4]. Successively, the structure was modified by adding a regular distribution of PEC spheres for the sake of exploring the effect of the inclusions on convergence. It turns out, as expected, that n_A is smaller if the inclusions are absent [13, Fig. 8].

Distance between the bricks The effect of this parameter was studied for general scattering problems that involved random clusters of different objects [11, Figs. 2, 5]. The outcome is that fewer ABFs are needed, if the average distance between the bricks is larger [11, Fig. 6].

Frequency Finally, the scattering from a collection of randomly distributed objects was studied in [13, Fig. 5] at different frequencies. By and large, the convergence patterns of a_s in [13, Fig. 9] suggest that at higher frequencies n_A increases.

As a complement to the numerical experiments outlined above, we have also examined the effect of ε_3 (see Fig. 1) on n_A. To this purpose, with the new code we have solved the scattering problem of a plane wave impinging on the dielectric structure shown in Fig. 3. The relevant LEGO model comprises $N_D = 8 \times 2 = 16$ bricks of two
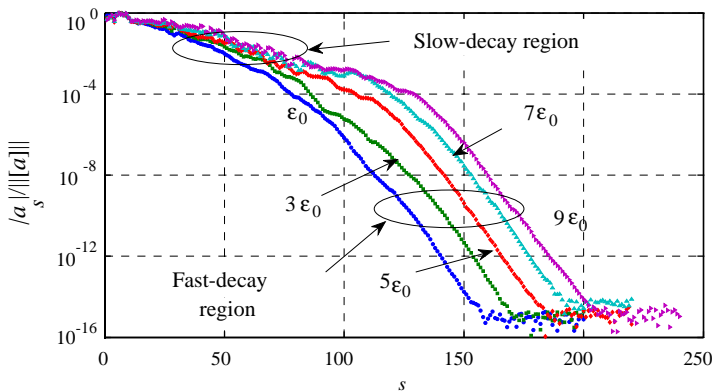
different types that are arranged in a regular checkerboard-like pattern as indicated. Type-1 (Type-2) bricks embed a large (small) cylindrical inclusion whose permittivity is increased in five discrete steps. The relevant geometrical and physical data for this simulation campaign are provided in the caption of Fig. 3.

The normalized current coefficients a_s are plotted in Fig. 4, where the parameter of the lines is the permittivity of the inclusions. It is
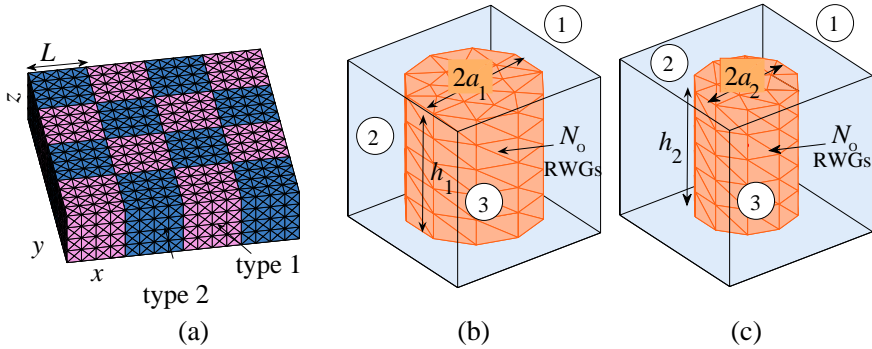
Figure 3. Dielectric slab with cylindrical holes or fillings for convergence analysis: (a) LEGO model with $N_D = 16$ cubic bricks; (b) close-up of the inside of type 1 brick; (c) close-up of the inside of type 2 brick. *Data*: $L = 10\,\mathrm{mm}$, $h_1 = h_2 = 8\,\mathrm{mm}$, $a_1 = 4\,\mathrm{mm}$, $a_2 = 3\,\mathrm{mm}$, $2N_F = 1152$, $N_O = 498$ (type 1), $N_O = 408$ (type 2), $f = 6\,\mathrm{GHz}$, $\mathbf{E}^i = \hat{\mathbf{y}}\exp(-jk_1 z)\,[\mathrm{V/m}]$, $k_1 = 2\pi f\sqrt{\varepsilon_1\mu_0}$, $\varepsilon_1 = \varepsilon_0$, $\varepsilon_2 = 11\varepsilon_0$, $\varepsilon_3 \in \{\varepsilon_0, 3\varepsilon_0, 5\varepsilon_0, 7\varepsilon_0, 9\varepsilon_0\}$.

Figure 4. Convergence pattern of the expansion coefficients a_s [see Eq. (4)] versus their index for the five case studies detailed in Fig. 3.

seen that a larger number of ABFs is required, if the contrast ratio $\varepsilon_3/\varepsilon_2$ is higher. One also realizes that the curves in Fig. 4 consist of two distinct regions of convergence (a circumstance also noticeable in the results of [12, 13]), which we dub slow- and fast-decay regions of the Arnoldi coefficients. The former is characterized by slow decay rate and possibly oscillations, whose amplitude and number seem to depend on the dielectric contrast between host medium and inclusions. In the fast-decay region, on the contrary, the a_s exhibit a steady and exponentially rapid decrease to zero with a slope that — in the present set of experiments — is somewhat independent of the actual value of ε_3. Besides, the onset of exponential decay is postponed for higher ratios $\varepsilon_3/\varepsilon_2$ until a critical value of n_A is attained. For instance, in case 1 ($\varepsilon_3 = \varepsilon_0$) the exponential decay rate kicks in at $n_A \approx 70$, whereas in case 5 ($\varepsilon_3 = 9\,\varepsilon_0$) it starts at $n_A \approx 130$.

To gain insights into the time requirements of LEGO, in Table 1 we have listed a few times relevant to the cases set up in Fig. 3. As the total number of computed ABFs was varied, it makes sense to compare the average time $\langle t_{ABF} \rangle$ taken to generate a single ABFs: such time is found to be approximately constant, in fact. The overall time t_{LEGO}, by contrast, increases with n_A. Finally, it is not superfluous to notice that the calculation of the transfer operators was performed *only once*, i.e., in correspondence with the first problem. A comparatively large amount of time can thus be saved by loading $[T_{kn}]$ from disk to analyze structures modelled with bricks whose position and shape are kept fixed.

4.3. Convergence of ABFs: Discussion

Admittedly, since so many parameters concur in determining the convergence pattern of a_s, it may not be possible to come up with a quantitative explanation of the behaviors observed so far. It may well

Table 1. CPU times[*] relevant to the cases detailed in Fig. 3.

ε_3	ε_0	$3\varepsilon_0$	$5\varepsilon_0$	$7\varepsilon_0$	$9\varepsilon_0$
n_A	200	200	220	220	240
$t_{T_{kn}}$ [min]	2.46	-	-	-	-
$\langle t_{ABF} \rangle$ [s]	1.96415	1.98170	1.90668	1.84331	1.96216
t_{LEGO} [min]	24.65[**]	22	22.52	26.03	25.42

[*] On a PC equipped with an Intel Core Quad CPU 2.66-GHz processor and 4-GB RAM

[**] This value includes $t_{T_{kn}}$

be the case, though, that the *eigenvalues* of $[T]\mathbf{diag}\{[S_{nn}]\}$ play a major role. In fact, all the parameters affect the eigenvalues of $[S_{nn}]$ (which in magnitude are smaller than unity [17]). On the other hand, the transfer operators $[T_{kn}]$ chiefly depend on the distance between the bricks. Furthermore, the ABFs are just but an orthonormal basis of the n_A-dimensional Krylov subspace spanned by the vectors $\{([T]\mathbf{diag}\{[S_{nn}]\})^{s-1}[q^i]\}_{s=1}^{n_A}$, which in turn form the Neumann series solution to the system. In this regard, although a series solution may not exist in general, the system is solvable and its solution can always be expressed as a linear combination of ABFs, as we just showed.

We *speculate* that (for a given level of accuracy) n_A depends on the specific form of spectrum of $[T]\mathbf{diag}\{[S_{nn}]\}$. More precisely, the smaller the eigenvalues, the fewer the ABFs required for the a_s to attain the threshold of numerical noise, and the faster the convergence rate (see Fig. 4). Conversely, the closer the eigenvalues are to the unit circle in the complex plane, the larger is n_A and correspondingly, the more delayed is the onset of the fast-decay region.

Lastly, we must mention that in [11], by means of extensive numerical experiments, we determined an approximate relationship linking the accuracy of the computed current coefficients $[q_{tot}^i]$ to the relative incremental difference δ_a defined in (5). Convenient and captivating as that relation can be, it appears to be less general than we had initially surmised. Tests conducted successively pointed out that it applies when the size of the bricks is in the neighborhood of the wavelength in the background medium[‡].

4.4. Choosing the Threshold for δ_a

In practical circumstances the best course of action is the adaptive generation of ABFs [11, Table 1]. Then, the question arises of how to choose the threshold against which δ_a is to be compared. In the light of (5) and the convergence curves of Fig. 4 one can argue that a smaller threshold most surely guarantees better accuracy of the solution, but obviously it also increases the computation time, because more ABFs need to be obtained.

We have found that setting the threshold at 10^{-5} affords a good tradeoff between accuracy and CPU-time. To substantiate this claim, we have solved the first scattering problem outlined in Fig. 3 with $\delta_a(n_A) = 10^{-5}$. This translates into $n_A = 85$ ABFs, the computation of which requires $t_{ABF} \approx 165\,\mathrm{s}$. In Fig. 5 the RCS thus computed is compared to the RCS obtained with $n_A = 200$ ABFs (which take $t_{ABF} \approx 393\,\mathrm{s}$ to calculate); the latter result can legitimately stand as a

---

[‡] Basically, all the cases addressed in [11] met this condition.
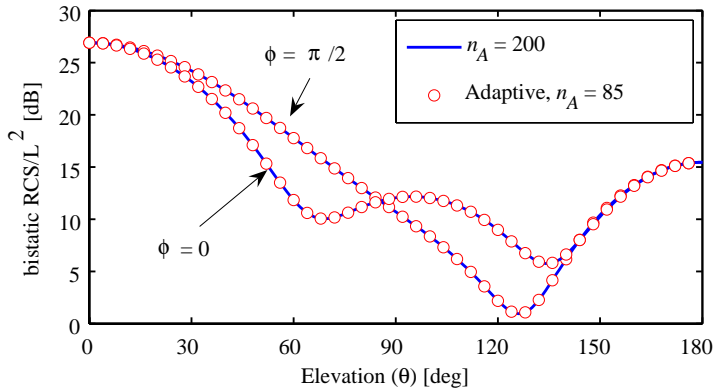
Figure 5. For testing the truncation criterion based on (5): the RCS of dielectric slab with cylindrical holes (first case defined in the caption of Fig. 3) obtained quitting the Arnoldi algorithm when $\delta_a = 10^{-5}$ ($\circ$) is compared to the results calculated using $n_A = 200$ ABFs (cf. Fig. 4).

reference in view of the pertinent convergence pattern of Fig. 4. As the two curves in Fig. 5 are undistinguishable for all practical purposes, this experiment demonstrates that $\delta_a(n_A) = 10^{-5}$ constitutes a viable choice.

5. CONCLUSION

By means of numerical examples we have discussed the convergence properties of the ABFs, which are employed to reduce the order of the LEGO algebraic system. Specific "rules of thumb" have been derived that can help predict how the number n_A of ABFs and the convergence rate of a_s will *relatively change*, in the event a certain physical or geometrical parameter is modified. Such information comes really handy when solving many similar EM scattering problems, in which one modifies one parameter at a time, e.g., in a design process. Nonetheless, since a general relationship that can *absolutely* predict n_A is not available, the adaptive generation of the ABFs constitutes a valid workaround. We have shown that quitting the Arnoldi algorithm when $\delta_a \approx 10^{-5}$ yields quite accurate results while saving on CPU-time.

ACKNOWLEDGMENT

The Authors would like to thank the Reviewers for their remarks.

REFERENCES

1. Peterson, A. F., S. L. Ray, and R. Mittra, *Computational Methods for Electromagnetics,* IEEE Press, Piscataway, 1998.

2. Harrington, R. F., *Field Computation by Moment Methods,* MacMillan, New York, 1968.

3. Kron, G., "A set of principles to interconnect the solutions of physical systems," *Journal of Applied Physics*, Vol. 24, No. 8, 965–980, 1953.

4. Matekovitz, L., V. A. Laza, and G. Vecchi, "Analysis of large complex structures with the synthetic-functions approach," *IEEE Trans. Antennas Propag.*, Vol. 55, 2509–2521, Sep. 2007.

5. Mittra, R. and K. Du, "Characteristic basis function method for iteration-free solution of large method of moments problems," *Progress In Electromagnetics Research B*, Vol. 6, 307–336, 2008.

6. Li, M.-K. and W. C. Chew, "Multiscale simulation of complex structures using equivalence principle algorithm with high-order field point sampling scheme," *IEEE Trans. Antennas Propag.*, Vol. 56, 2389–2397, Aug. 2008.

7. Xiao, G., J.-F. Mao, and B. Yuan, "A generalized surface integral equation formulation for analysis of complex electromagnetic systems," *IEEE Trans. Antennas Propag.*, Vol. 57, 701–710, Mar. 2009.

8. Lancellotti, V., B. P. de Hon, and A. G. Tijhuis, "An eigencurrent approach to the analysis of electrically large 3-D structures using linear embedding via Green's operators," *IEEE Trans. Antennas Propag.*, Vol. 57, 3575–3585, Nov. 2009.

9. Lancellotti, V., B. P. de Hon, and A. G. Tijhuis, "Scattering from large 3-D piecewise homogeneous bodies through linear embedding via Green's operators and Arnoldi basis functions," *Progress In Electromagnetics Research*, Vol. 103, 305–322, 2010.

10. Lancellotti, V., B. P. de Hon, and A. G. Tijhuis, "Linear embedding via Green's operators and Arnoldi basis functions for analyzing complex structures," *5th European Conference on Antennas and Propagation (EuCAP '11)*, 3519–3523, Rome, Italy, Apr. 2011.

11. Lancellotti, V., B. P. de Hon, and A. G. Tijhuis, "Wave scattering from random sets of closely spaced objects through linear embedding via Green's operators," *Waves in Random and Complex Media*, Vol. 21, 434–455, Aug. 2011.

12. Lancellotti, V., B. P. de Hon, and A. G. Tijhuis, "Linear embedding via Green's operators for 3-D scattering from piecewise

homogeneous bodies," *12th Int. Conf. on Electromagnetics in Advanced Applications (ICEAA '10)*, 349–352, invited paper, Sydney, Australia, Sept. 2010.

13. Lancellotti, V., B. P. de Hon, and A. G. Tijhuis, "A domain decomposition method for solving 3-D complex structures," *13th Int. Conf. on Electromagnetics in Advanced Applications (ICEAA '11)*, 195–198, invited paper, Turin, Italy, Sept. 2011.

14. Lancellotti, V., B. P. de Hon, and A. G. Tijhuis, "Scattering from a random distribution of numerous bodies with linear embedding via Green's operators," *AP/URSI Int. Symp.*, 650–653, Spokane, Washington, USA, Jul. 2011.

15. Rothwell, E. J. and M. J. Cloud, *Electromagnetics,* CRC Press, London, 2001.

16. Kurz, S. O. Rain, and S. Rjasanow, "The adaptive cross-approximation technique for the 3D boundary-element method," *IEEE Trans. Magn.*, Vol. 38, 421–424, Mar. 2002.

17. Lancellotti, V., B. P. de Hon, and A. G. Tijhuis, "On the convergence of the eigencurrent expansion method applied to linear embedding via Green's operators (LEGO)," *IEEE Trans. Antennas Propag.*, Vol. 58, 3231–3238, Oct. 2010.